Chinese Journal of Structural Chemistry

ARTICLE

Versatile Inorganic Oligomer-based Photochromic Spiropyrane Gels

Jiajia Song[1], Wei Duan[1], Yun Chen[1]* and Xiangyang Liu[2,3]*

[1]*State Key Laboratory of Chemo/Biosensing and Chemometrics, College of Chemistry and Chemical Engineering, Hunan University, Changsha 410082, China*

[2]*College of Ocean and Earth Sciences, College of Materials, College of Physical Science and Technology, State Key Laboratory of Marine Environmental Science (MEL), Research Institute for Biomimetics and Soft Matter, Xiamen University, Xiamen 361005, China*

[3]*Department of Physics, National University of Singapore, 2 Science Drive 3, Singapore 117542, Singapore*

ABSTRACT Here we report an example of a general strategy for the immobilization of various different photochromic spiropyran molecules on eco-friendly cheap nanomatrix. The spiropyrans are encapsulated in calcium salt oligomers-based gels by centrifugation, forming an inorganic oligomer-based gelatinous photoswitchable hybrid material. Ca^{2+} is also used to regulate the optical properties of spiropyrans through chelation. The oligomer-based gel can not only provide the space required for photoisomerization, but also reduce the interference of the surrounding environment on the photochromic properties. Moreover, a practical paper-based and colloidal flexible substrate platform is constructed for the removal and naked-eye detection of liquid and gaseous hydrazine at room temperature based on the reactivity of the formyl group on spiropyrans loaded in $Ca_3(PO_4)_2$ oligomers. This general strategy can be used for other inorganic oligomer-based molecular switches and sensing systems.

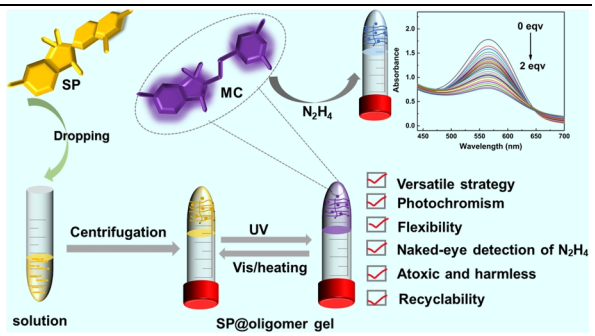

Keywords: inorganic oligomer, photochromic, gels, naked-eye detection of hydrazine

n INTRODUCTION

Spiropyrans are one of the most extensively investigated light stimuli-responsive switchable molecules. They can undergo a reversible isomerization between the colorless spirocyclic (SP) form and the colored merocyanine (MC) form based on the cleavage and formation of the C_{spiro}-O_{pyran} bond with light excitation.[1] Additional external inductive stimuli such as ion-driven,[2] temperature[3] or pH changes[4] are also often required. Obviously, this isomerization reaction needs conformational transition freedom, which makes the switching function of spiropyran molecule subject to the crystal lattice and the steric obstacle in solid state.[5,6] Thus, most of the past spiropyran studies were focused on solution systems. Recently, efforts on harbouring spiropyran molecules within polymers[7-9] and the nanocavities in metal organic[10-14] and covalent organic frameworks[15,16] (MOFs and COFs) are making exhilarating progress. However, it is often not easy to design and synthesize large numbers of complicated MOFs and COFs to fit various dye molecules with different sizes and shapes.[17] The recycling of both dyes and carriers will also be tedious and complicated. Therefore, it is of great importance to find convenient versatile alternative carrying system to satisfy various different photochromic molecules.

As a flexible soft material with a spatial network structure, eco-friendly cheap inorganic oligomer-based hybrid gels are arguably excellent candidates for spiropyrans with great application potential.[18,19] Various responsive recognition entities can be easily integrated into the versatile gelatinous nanostructure scaffold by simple metal-probe coordination processes and centrifugation methods. Flexible cavities and weak intermolecular interaction facilitate the specific responses and the entries of small molecules. It can be predictable that these inorganic oligomer-based gelatinous photoswitchable hybrid materials have extensive advantages such as versatility, simple operation, wide applicability, long-acting, less dye consumption, eco-friendly, recyclability and low cost. In this work we encapsulated the spiropyran molecules in oligomers matrix and obtained the spiropyrans@calcium ionic oligomer colloids by centrifugation. Compared with the conventional solid substrate, colloidal oligomers can not only provide enough space for the photoisomerization of spiropyran molecules, but also avoid the self-quenching caused by molecular aggregation. Calcium ionic oligomer is atoxic and harmless with good biocompatibility and ductility. In addition, inspired by the detection platform for formaldehyde[20-22] based on the acylation reaction of formaldehyde and hydrazine, we expect to construct the paper-based and colloidal flexible substrate platform for naked-eye detection of liquid and gaseous hydrazine at room temperature, which is an important highly reactive compound,[23] but is easily absorbed into the human body through the respiratory system, digestive system and skin to damage the central nervous system, corrode skin and internal organs, and even to induce cancer.[24] Compared with the traditional hydrazine detection methods in solution system, the naked-eye sensors based on solid-substrate have the advantages of low cost, operability, portability and real time. In short, although imperfect, we provide here a general strategy that can be used for many inorganic oligomer-based molecular switching and sensing systems.

n RESULTS AND DISCUSSION

Four colloidal oligomer optical switching systems SC-FSP@

DOI: 10.14102/j.cnki.0254-5861.2022-0061

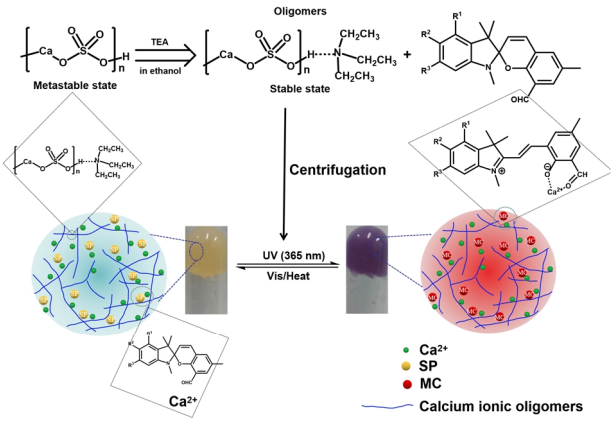

Scheme 1. Diagrammatic sketching of the preparation of calcium ionic-induced photochromic colloidal spiropyrans@$CaSO_4$ nano-oligomers (FSP: $R^1 = R^2 = R^3 = H$; SC-FSP: $R^1 = R^3 = H$, $R^2 = COOH$; DC-FSP: $R^1 = R^3 = COOH$, $R^2 = H$. Green spheres represent free Ca^{2+} in oligomers. The left and right insets are the photographs of the spiropyrans@oligomers before and after UV radiation taken in the experiment. The preparation schematic diagram of spiropyrans@$Ca_3(PO_4)_2$ oligomers is not given, but it is similar to that shown in the above scheme).

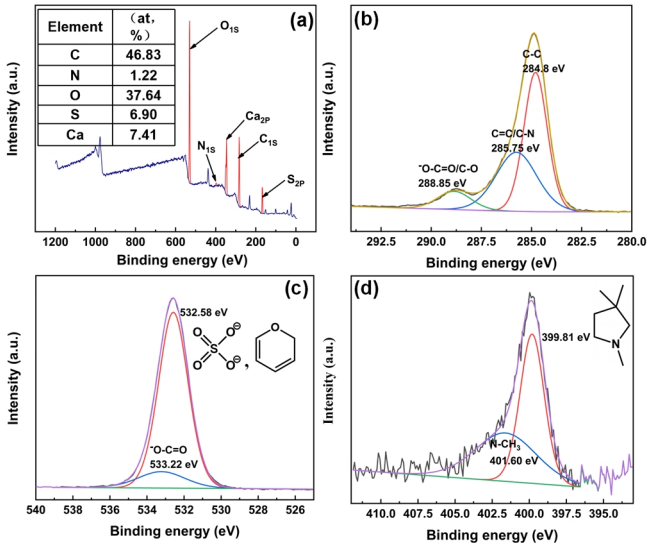

Figure 2. (a) XPS survey spectrum of SC-FSP@$CaSO_4$ oligomers (The atomic percentage is showed in the upper left table). The decomposition peaks of C 1s, O 1s and N1s obtained by high-resolution scanning are shown in (b)-(d), respectively.

$CaSO_4$, SC-FSP@$Ca_3(PO4)_2$, DC-FSP@$Ca_3(PO4)_2$ and FSP@$Ca_3(PO4)_2$ were obtained by integrating spiropyrans into the pre-prepared oligomer solutions of calcium phosphate and calcium sulfate through simple physical blending with triethylamine as the capping stabilizing agent. Scheme 1 displays the preparation and chromogenic mechanism of gel-like spiropyran@calcium ionic oligomers. In addition to building oligomers, calcium ions therein are also used to induce the isomerization of spiropyrans, so as to improve the photochromic performance of spiropyran molecules in general. Trisethylamine is used as the capping stabilizing agent to stabilize nano-oligomers because its nitrogen atom can form hydrogen bonds with protonated phosphate or sulfate, promoting linear growth of the nano-oligomers.[25] The curing of spiropyran molecules is realized by directly doping crosslinking calcium ionic oligomers. The colloidal spiropyran@calcium ionic oligomers are obtained by centrifugation. On one hand, spiropyran molecules are encapsulated in oligomers matrix to avoid the influence of the external environment (polarity of solvent, pH value, acid, alkali, etc.),[26] so as to effectively improve the environmental tolerance. On the other hand, compared with solid matrix, the colloid oligomers can provide sufficient space for the photoisomerization of spiropyran molecules, thereby improving the photochromic performance and cycle endurance.

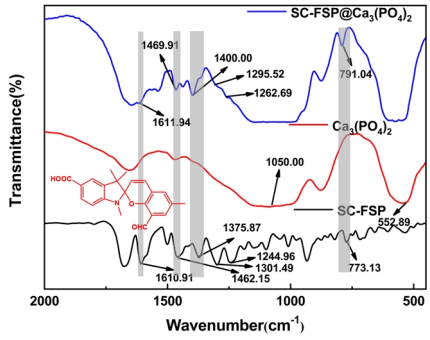

Figure 1. FTIR spectra of SC-FSP@$Ca_3(PO4)_2$ oligomers.

Characterization of the Spiropyrans@calcium Ionic Oligomers. As shown in Figure 1, the FTIR data indicate that spiropyran molecules are successfully embedded into calcium oligomers (Figure 1 and S1). Peaks at 1050 and 552 cm^{-1} originate from the skeleton stretching vibration of Ca-P-O and the stretching vibration of P=O, respectively. Compared with the initial calcium phosphate, several new absorption bands belonging to spiropyran SC-FSP appear in the wavelength range of 1700-500 cm^{-1} for the functionalized SC-FSP@$Ca_3(PO4)_2$. The peaks at 1611 and 791 cm^{-1} are related to the skeleton vibrations of benzene ring and the out-of-plane bending vibrations of the aromatic C-H, respectively. The existence of methyl groups is confirmed by the stretching vibration absorption peaks of C-C bonds at 1469 and 1400 cm^{-1}. The vibrational band corresponding to Ar-O-C stretching is found at 1262 cm^{-1} and the vibrational frequency of C-N bond of the indole cycle presents itself at 1295 cm^{-1}. Similarly, the characteristic bands are also found at 1459 and 1561 cm^{-1} for DC-FSP@$Ca_3(PO4)_2$ and FSP@$Ca_3(PO4)_2$, respectively (Figure S1a-b) due to the benzene ring skeleton stretching.

The successful embedding of spiropyrans in calcium oligomers was further confirmed by XPS technique. Taking SC-FSP@$CaSO_4$ system as an example, the C 1s, O 1s and N 1s peaks attributed to spiropyran SC-FSP can be found at 283, 530 and 398 eV, respectively (Figure 2a). The decomposition peaks of C1s, O1s and N1s show that spiropyrans embedded in $CaSO_4$ oligomer still exist in ring-closed SP form under the test conditions. The C1s spectrum consists of three peaks (Figure 2b), among which the peak at 285.75 eV originates from C=C and C-N in spiropyran (ring-closed form).[27] The peak at 288.85 eV originates from C-O of pyran ring and carboxyl carbon[28,29] in SP. For the O 1s spectrum (Figure 2c), the peak at 532.58 eV is the characteristic band

DOI: 10.14102/j.cnki.0254-5861.2022-0061

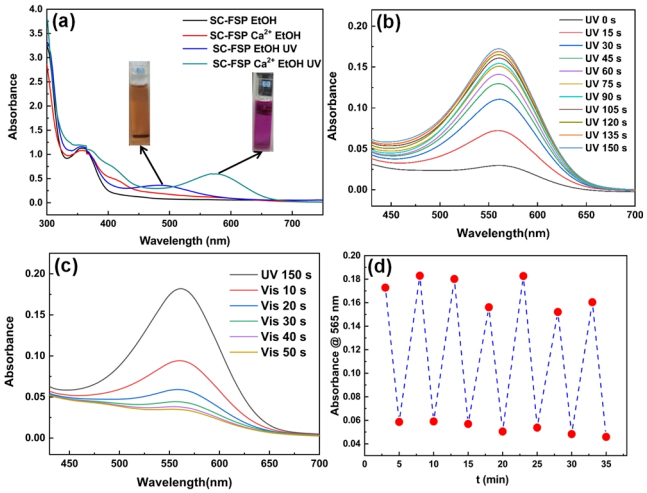

Figure 3. (a) The effect of Ca^{2+} on the optical switching behavior of SC-FSP. Variation of the absorption spectra of SC-FSP (25.76 μM) in ethanol solution containing Ca^{2+} (30 mM) after irradiation with ultraviolet light (b) and visible light (c) for different periods of time. (d) The fatigue resistance test of SC-FSP in Ca^{2+} ethanol solution by alternate irradiation with UV for 3 min and Vis for 2 min.

of O-C on pyran ring in spiropyrans and O 1s in $CaSO_4$. The binding energy at around 399.81 eV shown in Figure 2d is ascribed to amine nitrogen, which also confirms the existence of ring-closed spiropyran form. The decomposition peaks of S 2p and Ca 2p in SC-FSP@$CaSO_4$ oligomer are described in Figure S2 in the Supporting Information.

The microscopic topography observation of SC-FSP@$CaSO_4$ oligomer was carried out by Scanning Electron Microscope (SEM, Hitachi S-4800, Japan). Several drops of diluted sample were placed on the silicon wafer and dried at 50 °C under vacuum for 1 hour. The morphology of the sample is linear as shown in Figure S3(a). This trend can be explained by that the volatilization of triethylamine leads to the crosslinking of oligomers during the drying of SC-FSP@$CaSO_4$ oligomers solution, promoting the formation of the mineral phase calcium sulfate and SC-FSP composites. The average length and width of the sample are 8.77 and 1.04 μm (Figure S3b & c), respectively, obtained from the statistical analysis of more than 100 samples. The uniform integration of spiropyran molecules SC-FSP into the linear $CaSO_4$ composite is also confirmed by EDS analysis (Figure S3d-h).

Regulation of Ca^{2+} on Photochromic Behavior of Spiropyrans in Oligomers. Before studying the photochromic properties of spiropyran@calcium ionic oligomers, it is necessary to investigate the role of Ca^{2+} in the isomerization regulating and the coloration mechanism of spiropyrans integrated into gel-like oligomers. Figure 3a shows the effect of Ca^{2+} on the UV absorption spectra of SC-FSP in ethanol solution. It can be found that when SC-FSP without Ca^{2+} is irradiated by ultraviolet light (365 nm), the visible absorption peak of isomeric merocyanine (MC) appears at about 485 nm due to the photoisomerization from the ring-closed spiropyran form (SP) to the ring-opened merocyanine form (MC). Subsequently, by the introduction of Ca^{2+} into the SC-FSP solution,

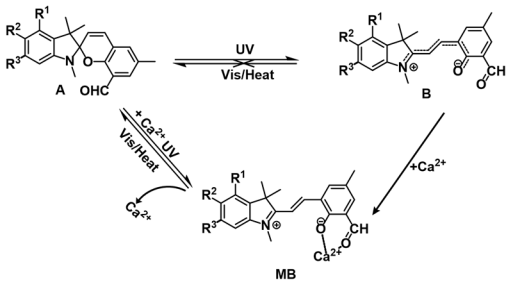

Figure 4. The coloration mechanism of spiropyran molecules integrated into colloidal calcium ionic oligomers (FSP: $R^1 = R^2 = R^3 = H$; SC-FSP: $R^1 = R^3 = H$, $R^2 = COOH$; DC-FSP: $R^1 = R^3 = COOH$, $R^2 = H$).

an obvious red shift of the maximum absorption wavelength to 565 nm is observed. After photo-induced isomerization reaction, the color of the solution also changes from orange to fuchsia. Interestingly, SC-FSP in ethanol solution can reversibly undergo photoisomerization reaction by the regulation of Ca^{2+}. As shown in Figure 3b, the absorption band intensity at 565 nm increases by prolonging the UV radiation time (15 s intervals) and the conversion rate of SP to MC reaches its maximum after 2.5 minutes. In addition, by stepwise irradiation of visible light (10 s intervals), the MC′ absorption intensity at 565 nm gradually decreases to the minimum after 50 s (Figure 3c). When the sample is alternately exposed to ultraviolet light (365 nm, 3 min) and visible light (2 min), from Figure 3d we can see that the SC-FSP still performs acceptable resistance to photo-degradation after 7 cycles in Ca^{2+} ethanol solution. However, when there is no Ca^{2+} in SC-FSP solution, it exhibits an irreversible photochromic process. The MC cannot be transformed into SP again after photoisomerization, no matter under visible light radiation or heating conditions. This is because zwitterionic merocyanine is easy to form aggregation state in solution due to its large dipole moment, which improves the stability to a certain extent.[30] Similarly, the photoisomerization properties of FSP and DC-FSP can also be regulated by Ca^{2+}. For FSP, when it is exposed to UV light, Ca^{2+} causes red-shift of λ_{max} of the ring-opened MC from 470 to 550 nm. The decolorization isomerization of MC→SP can reversibly occur with visible light irradiation again. In contrast, this process is irreversible without Ca^{2+} (Figure S4a). DC-FSP exists stably in the form of ring-closed SP in ethanol solution. It cannot undergo SP→MC ring-opening isomerization reaction with UV radiation, probably because electron-withdrawing carboxyl groups on the indoline reduce the stability of zwitterionic merocyanine in ethanol. While the C_{spiro}–O bond can be cleaved driven by ultraviolet radiation with the appearance of maximum absorption peak of merocyanine at 550 nm from the regulation of Ca^{2+} (Figure S4b). Fatigue resistance experiments carried out by alternate exposure to ultraviolet and visible light show that FSP and DC-FSP have the potential as available optical switches in Ca^{2+} ethanol solution due to their photodegradation durability basically in line with expectations (Figure S5).

There is a large number of excess free Ca^{2+} in our colloidal photoswitching systems, and their regulation on the photochromic properties by chelating spiropyrans can be confirmed by the UV-

DOI: 10.14102/j.cnki.0254-5861.2022-0061

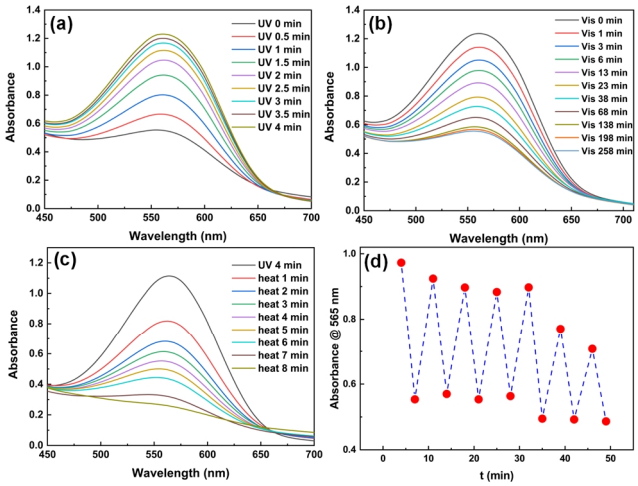

Figure 5. Photo-response behavior of colloidal SC-FSP@$Ca_3(PO_4)_2$ oligomers. The time-dependent absorption spectra at 565 nm irradiation with ultraviolet light (a), visible light (b) and heated in a water bath at 50 °C (c). (d) Photodegradation-durability of the colloidal SC-FSP@$Ca_3(PO_4)_2$ oligomers by alternate irradiation with UV for 4 min and heated in 50 °C water bath for 8 min.

Vis absorption spectra of spiropyrans in ethanol solution with Ca^{2+}. It has also been reported[31] that the phenolate anion of merocyanine structure can be reversibly photochemically chelated with the Ca^{2+} bound to the diazacrown ether up to construct chromogenic sensor of Ca^{2+}. Mutsuo Tanaka et al.[32] found that spiropyrans containing monoazathiocrown ethers showed negative photochromism due to the thermal isomerization induced by Ca^{2+} interaction with phenolate anion of the merocyanine form. In our study, as shown in Figure 4, the presence of formyl group on pyran ring in SP molecules provides a chelating site for Ca^{2+}. Under the stimulation of ultraviolet light, Ca^{2+} can coordinate with the phenolate anion of MC, formyl oxygen, and solvent ethanol molecules. Because electron-withdrawing carboxyl groups on benzene ring in indolin are not conducive to the thermal stability of the zwitterionic merocyanine structure, the spiropyran@calcium ionic oligomers are induced to show positive photochromism. Under ultraviolet radiation, colorless ring-closed SP isomerizes into the colored zwitterionic MC due to the heterotic cleavage of C-O bond, and MC can be reversibly transformed into SP under visible light or heating conditions.

Stimulus-responsive Behavior. The photochromic behaviors of the oligomers with spiropyrans were researched by UV-Vis absorption spectra, suggesting that they performed reversible photo-responsiveness under the light illumination with different wavelengths. Optimization experiments on the amount of SC-FSP embedded in $Ca_3(PO_4)_2$ oligomers show that the photochromic performance of SC-FSP@$Ca_3(PO_4)_2$ photoswitch is concentration-dependent. Insufficient spiropyran molecules cannot offer the colloidal oligomers optimum photo-response characteristics. If excessive spiropyran molecules are integrated into the limited space of colloidal matrix, it would hinder the photoisomerization reaction and result in poor photofatigue resistance. Moreover, the interca-

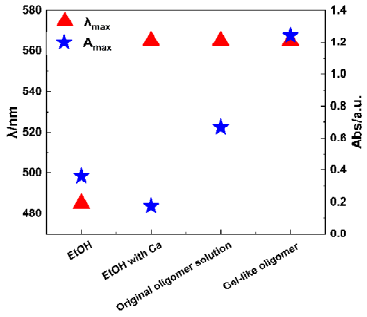

Figure 6. Comparison of λ_{max} and A_{max} of SC-FSP (25.76 μM) in four matrices (ethanol solution, ethanol solution with 30 mM Ca^{2+}, original $Ca_3(PO_4)_2$ oligomer solution and colloidal $Ca_3(PO_4)_2$ oligomers) in the ultraviolet-visible absorption spectra.

lation of excessive spiropyrans would induce thermal isomerization in the presence of Ca^{2+}, resulting in the conversion of SP to MC even without UV illumination. As shown in Figure S6, according to the comparison of absorbance difference at 565 nm before and after UV radiation for 15 min, spiropyrans SC-FSP with a concentration of 25.76 μM were finally integrated into $Ca_3(PO_4)_2$ oligomers. The SC-FSP@$Ca_3(PO_4)_2$ oligomer sample obtained by centrifugation was evenly coated on the surface of the quartz cuvette, and researched by UV-Vis spectra under multiple UV irradiation within 4 min in 30 s intervals. Triggered by ultraviolet light, the spiropyrans-oligomers photoswitch was photoisomerized from spiro (SP) to merocyanine (MC) forms. It was characterized in that the absorption peak of MC appeared at 565 nm due to photochromism (Figure 5a). Figure 5b-c display that SC-FSP@$Ca_3(PO_4)_2$ oligomers can reversibly isomerize from opened-ring colored MC form to closed-ring colorless SP form under visible light illumination or heating conditions along with the absorbance at 565 nm up to the minimum.

The anti-photodegradation ability and photochromic reversibility of SC-FSP@$Ca_3(PO_4)_2$ oligomers were further studied by alternately irradiated with UV for 4 min and heated in 50 °C water bath for 8 min. SC-FSP@$Ca_3(PO_4)_2$ oligomers can realize reversible conversion between spiro (SP) and merocyanine (MC) forms. Figure 5d shows the absorbance at 565 nm related to MC isomers decreases to 73% after 7 cycles. The slight decrease may be due

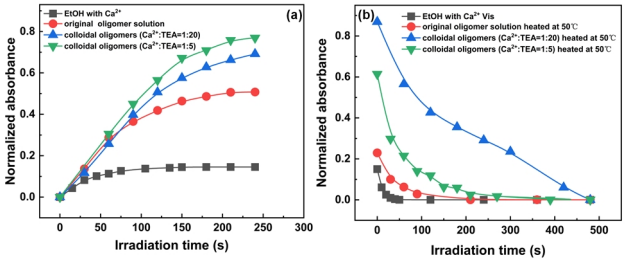

Figure 7. The absorbance of spiropyran SC-FSP at 565 nm versus (a) UV (365 nm) irradiation time for SP conversion to MC and (b) Vis irradiation or heating time for MC conversion to SP in different matrix environments (ethanol solution with 30 mM Ca^{2+}, original $Ca_3(PO_4)_2$ oligomer solution and colloidal $Ca_3(PO_4)_2$ oligomers).

DOI: 10.14102/j.cnki.0254-5861.2022-0061

to the crosslinking of oligomers triggered by the volatilization of small amount of capping agent in the process of decoloration isomerization by heating, so that the isomerization from SP to MC is subjected to steric effects a certain extent. Not only the free Ca^{2+} in the oligomers can regulate the optical properties of spiropyrans, but also the colloidal matrix ensures the space required for its isomerization and avoids the interference of the surrounding environment of spiropyran molecules in solution on photochromic performance. As the most common inorganic salt in nature, calcium salt is atoxic and harmless with good biocompatibility. Therefore, the spiropyran@calcium ionic oligomers obtained by this strategy also has potential application value in the field of controlled drug delivery systems as a kind of photoswitch.

The maximum absorption intensity was closely related to the surrounding environment of spiropyran molecules and oligomer states. As shown in Figure 6, the λ_{max} and A_{max} of SC-FSP (25.76 μM) upon triggering with UV light were compared in ethanol solution, original $Ca_3(PO_4)_2$ oligomer solution and $Ca_3(PO_4)_2$ colloidal oligomers. It can be observed that in addition to the red-shift of λ_{max} under the regulation of Ca^{2+}, the colloidal oligomer matrix resulted in higher photochromic intensities of spiropyrans. The A_{max} characteristic of MC was significantly higher than that in original oligomer solution and ethanol solution. On one hand, the matrix density of spiropyrans in colloidal oligomers was increased by centrifugation. Another reason was that the colloidal matrix relatively increased the steric hindrance of decolorization isomerization from MC to SP, thus enhancing the thermal stability of chromogenic MC, which was also confirmed by the kinetic study of photoisomerization process. The photoresponse behavior of SC-FSP in original $Ca_3(PO_4)_2$ oligomer solution is shown in Figure S7.

Furthermore, three spiropyrans integrated into $Ca_3(PO_4)_2$ oligomers were quantitatively analyzed by UV-Vis spectroscopy in order to further investigate their photochromic behavior. Specifically, the absorption spectra of spiropyrans with different concentrations in ethanol solution with Ca^{2+} were measured by UV-Vis spectrophotometer (Figure S8a and S9a). The calibration curves were drawn according to the function of the absorbance at λ_{max} and the concentration (Figure S8b and S9b). Afterwards, the absorption spectra of residual spiropyrans in the supernatant of colloidal oligomers after centrifugation were recorded. The contents of spiropyrans embedded in the colloidal oligomers were determined by subtracting the remaining content in the supernatant from the total spiropyran content. Thus, the embedding amounts of FSP, SC-FSP and DC-FSP can be calculated as 65.9%, 93.8% and ~100% of the total, respectively (shown in Table S1). The FSP@$Ca_3(PO_4)_2$ and DC-FSP@$Ca_3(PO_4)_2$ colloidal oligomers prepared by the same method also performed acceptable photochromic behavior. As shown in Figure S10(a), the absorbance at 550 nm of DC-FSP@$Ca_3(PO_4)_2$ gradually grew up with the increase of UV radiation time (30 s intervals), demonstrating more SP converted to MC. Figure S10(b) shows MC could be reversibly isomerized to SP upon heating. Compared with the decoloration isomerization process of SC-FSP@$Ca_3(PO_4)_2$ colloidal oligomers, obviously, the conversion rate from MC to SP for DC-FSP@$Ca_3(PO_4)_2$ oligomers was slower at the same temperature. After heating for 15 min, the absorption intensity at 550 nm basically remained stable and only decreased by 37%, indicating that DC-FSP still mainly existed in MC form in $Ca_3(PO_4)_2$ oligomers. This may be because more DC-FSP molecules were embedded in $Ca_3(PO_4)_2$ oligomers than SC-FSP, which increased the spatial hindrance effect of MC isomerization to SP. The colloidal FSP@$Ca_3(PO_4)_2$ oligomer was repeatedly treated with UV (365 nm, 5 min) and water bath (50 °C, 15 min) for 8 cycles. The absorbance at 540 nm after each treatment was displayed in Figure S11, finding the FSP@$Ca_3(PO_4)_2$ has inferior anti-photodegradation ability during this period.

For the purpose of investigating the influence of calcium ionic oligomers on the photoisomerization rate of spiropyran SC-FSP embedded in it, the absorbance at 565 nm versus UV (365 nm) irradiation and heating time were recorded in different matrix environments (ethanol solution with Ca^{2+}, original oligomer solution and colloidal oligomers). During the isomerization from SP to MC under UV radiation, the speed of arriving the equilibrium point in ethanol solution with Ca^{2+} was slightly faster than that in oligomer solution and colloidal oligomers (Figure 7a). This may be due to the relatively larger intermolecular space in ethanol solution, which is conducive to the transformation from SP to MC. On the other hand, the spectra also described that the MC has the high-

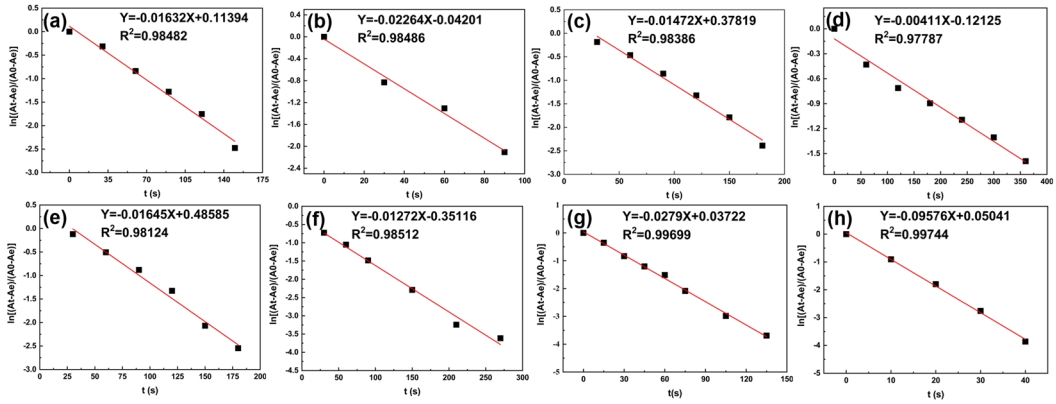

Figure 8. Kinetic fitting curves of SC-FSP in original $Ca_3(PO_4)_2$ oligomer solution (a & b), colloidal $Ca_3(PO_4)_2$ oligomers with $n(Ca^{2+})$:n(TEA) = 1:20 (c & d) and 1:5 (e & f), ethanol solution with 30 mM Ca^{2+} (g & h). The coloration isomerization of SP to MC stimulated by UV light (a, c, e & g). The decoloration isomerization of MC to SP heated in a 50 °C water bath (b, d & f) or Vis irradiation (h).

DOI: 10.14102/j.cnki.0254-5861.2022-0061

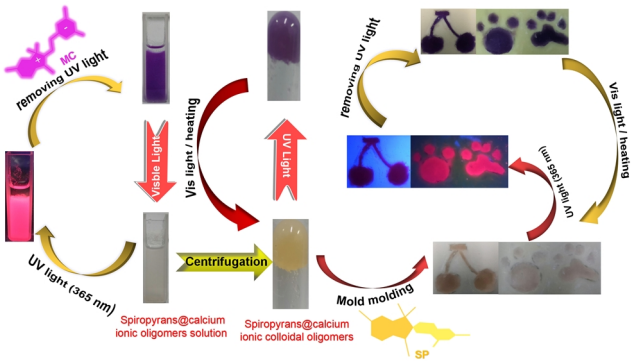

Figure 9. The fluorescent and photochromic properties of functional calcium ionic oligomers containing spiropyrans in the emulsive states and colloidal states.

est absorbance value after UV illumination in colloidal oligomers because of the largest matrix density. For the photochemical process of MC to SP (Figure 7b), the spectra showed that the speed of reaching the equilibrium point was the fastest in ethanol solution, followed by the original oligomer solution, and the slowest in colloidal oligomers. In addition, the preliminary exploration found that the content of capping agent in the oligomers may also affect the isomerization rate of SC-FSP. Compared with the oligomers with $n(Ca^{2+})$:n(TEA) of 1:5, the rate of MC isomerization to SP is much slower in the oligomers with the ratio of 1:20. The reason may be that the increase of the proportion of capping agent led to the reduction of the size of nanoclusters. The isomerization space of spiropyrans embedded in it was limited, so it was not conducive to the conversion of MC.

The spectra in Figure 7 show that the isomerization rate of all samples is exponentially related to time. The *A*-*T* curves were fitted by taking $\ln\frac{A_t-A_e}{A_0-A_e}$ as ordinate and t as abscissa to further study the isomerization kinetics of SC-FSP in different matrix environments, as shown in Figure 8. It can be seen that the kinetics of coloration and decoloration isomerization basically accorded with the linear relationship, indicating that the photochemical process of SC-FSP corresponded to the first-order kinetic equation, namely, $\ln(A_t - A_e) = -K_c t + \ln(A_0 - A_e)$.[33] K_c expresses the rate constant of isomerization reaction, which can well indicate the response of SC-FSP@calcium ionic oligomers to UV radiation and temperature during the process of photoisomerization. A_0, A_t and A_e are the absorbance values at 565 nm at the beginning, time t and end of photochemical reaction extracted from Figure 7, respectively. The fitted kinetic equations and related parameters such as K_c, R^2 (correlation coefficient) and $T_{1/2}$ (time needed to reach half of the ultimate absorbance of coloration and decoloration) are listed in Table S2 (Supporting Information), according to which, upon UV radiation, the colorization rate of SC-FSP in ethanol solution with Ca^{2+}, original oligomer solution and colloidal oligomers with $n(Ca^{2+})$:n(TEA) of 1:5 and 1:20 are 2.79×10^{-2}, 1.63×10^{-2}, 1.65×10^{-2} and 1.47×10^{-2} s^{-1}, respectively. As mentioned earlier, SC-FSP has a faster isomerization rate in ethanol solution. For the decoloration isomerization process under heating conditions, the rate constants are 9.58×10^{-2} s^{-1} (vis radiation), 2.26×10^{-2}, 1.27×10^{-2}, and 4.11×10^{-3} s^{-1}, respectively. The spiropyrans embedded in oligomers possessed lower decolorization speed than that in ethanol solution due to the reduction of free volume required for isomerization rotation. Moreover, the increase of proportion of capping agent may reduce the size of nanoclusters, and therefore the oligomers produced a slower decolorization responsivity to temperature stimulation.

In order to explore the potential applications of the calcium ionic oligomer colloids containing spiropyrans in optical information storage and anti-counterfeiting technology as a photosensitive ink, the photo-patterning ability and photochromic property were investigated by photography. Color changes before and after the reversible photoisomerization behavior of spiropyrans in oligomer colloids can be observed with naked eyes. Therefore, through simple casting of oligomer colloids, various recorded patterns can be easily depicted with the stimulation of UV-light source. As shown in Figure 9, both the original oligomer solution and the colloids obtained by centrifugation showed high-intensity red fluorescence and the characteristics of photochromism upon and after UV excitation, respectively. As expected, since spiropyran molecules stably existed in the colorless SP form before UV irradiation, the drawn patterns presented decolorized states. After UV-light excitation (20 s), the closed-ring SP structure immediately photoisomerized into the opened-ring MC structure and the recorded patterns performed visible coloration states with red fluorescence. Compared with ordinary inks that only emit fluorescence under excitation with UV-light, the calcium ionic oligomer colloids simultaneously exhibit both photochromism and high-intensity fluorescent emission under UV illumination. The observation results confirm that the photochromic calcium ionic oligomer colloids have the potential to be developed as an anti-counterfeiting material with multiple security levels.[34,35]

Naked-eye Detection and Mechanism Study of Liquid and Gaseous Hydrazine on the Paper and Soft Substrates. Hydrazine is extensively used in the fields of chemistry,[36,37] medicine,[38] agriculture,[39] rocket fuel,[40] water treatment,[41] photography and so on,[42] but is also highly toxic. In order to verify the feasibility of the principle based on the acylation reaction of formyl in spiropyrans with hydrazine for naked-eye sensing of hydrazine, the photoresponse of spiropyrans towards hydrazine was studied in the original $Ca_3(PO_4)_2$ oligomer solution. As shown in Figure 10,

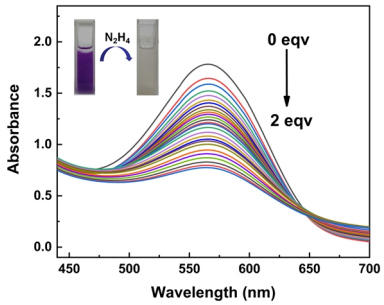

Figure 10. The changes of UV-Vis absorbance spectra of SC-FSP (100 μM) in $Ca_3(PO_4)_2$ oligomer solution with the dropping of N_2H_4 (0-2 equiv.) during the titration experiments. Inset: the visual color of SC-FSP@$Ca_3(PO_4)_2$ oligomer solution observed before and after the titration experiment.

DOI: 10.14102/j.cnki.0254-5861.2022-0061

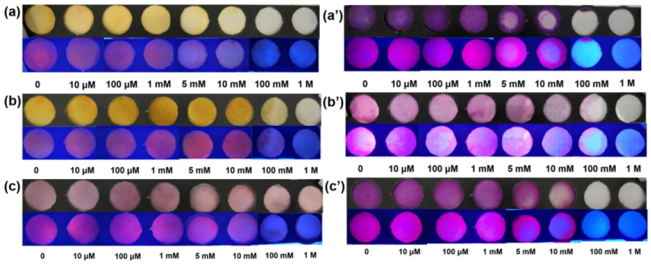

Figure 11. The color changes of filter paper pretreated with spiropyrans (9.2 mM) after dropping ethanol solutions of different hydrazine concentrations. Upper row: visual color observed under ambient visible light. Lower row: fluorescent color observed under UV light. (a) SC-FSP, (a′) SC-FSP-Ca^{2+}, (b) DC-FSP, (b′) DC-FSP-Ca^{2+}, (c) FSP, (c′) FSP-Ca^{2+}.

the UV-Vis spectra exhibited that the maximum absorption of the ring-opening MC form for SC-FSP (c = 100 μM) appeared at about 565 nm. The maxima gradually decreased with the addition of hydrazine (0.5 M in ethanol solution). The color of oligomer solution changed from purple to colorless, which provided the possibility to detect hydrazine with the naked eyes. Similarly, the absorbance of DC-FSP and FSP at 550 nm also decreased due to the reaction with hydrazine, accompanied by the change of oligomers solution color from purple to colorless (Figure S12).

The spiropyrans in $Ca_3(PO_4)_2$ oligomer solution are feasible for colorimetric sensing of hydrazine by the above analysis. We further studied the naked-eye colorimetric and fluorescent responses on the paper substrate. The filter paper was used as the substrate for the construction of liquid hydrazine sensor. Firstly, spiropyrans were coated on the filter paper by soaking the filter paper strips in ethanol solutions of SC-FSP, DC-FSP and FSP (9.2 mM) with or without Ca^{2+} for 2 min and drying, respectively. As shown in the upper rows in Figure 11a-c, SC-FSP, DC-FSP and FSP displayed light yellow and red in the absence of Ca^{2+} and N_2H_4 under ambient visible light. When the filter paper was immersed in ethanol solution with Ca^{2+} and dried, the color of the filter paper before the addition of N_2H_4 was dark purple due to the photoisomerization of spiropyrans from SP form into MC form induced by Ca^{2+} (upper rows of Figure 11a′, b′ and c′). Then, hydrazine ethanol solutions with different concentrations were dropped onto the filter paper and dried naturally. It could be found that the color of the filter paper gradually faded with the hydrazine concentrations from 10 μM to 1 M, and under UV irradiation the fluorescent color also changed from red to bluish-purple. When the hydrazine concentration was 5 mM, the color change of SC-FSP could be recognized by the naked-eye observation shown in Figure 11a and a′. DC-FSP and FSP also experienced emissive color changes from red to bluish-purple (lower rows of Figure 11b, b′, c and c′). By comparison, it can be concluded that SC-FSP is much more sensitive than DC-FSP and FSP on solid paper-substrate, which makes SC-FSP have a wider responsive range for naked-eye detection of hydrazine through the colorimetric and fluorescent changes.

As a kind of “wet and soft” material, calcium ionic oligomer colloids have many advantages, such as innocuity, flexible shapes and good biocompatibility. Therefore, integration the stimulus-responsive spiropyran into its colloidal structures can be used to develop flexible intelligent sensors. Here, based on $Ca_3(PO_4)_2$ oligomer colloidal substrate, SC-FSP was selected to detect gaseous hydrazine. The SC-FSP@$Ca_3(PO_4)_2$ oligomer colloid ($C_{SC\text{-}FSP}$ = 25.76 μM) was obtained by centrifugation. Under UV light stimulation, the spiropyrans loaded in the colloid were photoisomerized to ring-opened MC form and the colloid was induced to turn purple (see the first photo in Figure 12). Then the purple colloid was smeared on the foam and placed on the top of the bottles containing different concentrations of aqueous solution of hydrazine (3 mL, concentrations: blank, 0.1%, 1%, 5%, 10%, 15%, 20%, 30%, 40%, 70% and 100%) and other analyte aqueous solutions for one hour at room temperature. With the increasing of hydrazine, the change extent of color for colloidal substrate was gradually increased. Finally, the visual colors of colloids gradually turned from purple to colorlessness and the emissive color changed from red to bluish-purple, as shown in Figure 12. It can be found that the color changes can be distinguished by the naked-eye when the amount of hydrazine increases to 10%. In addition, the visible and fluorescent colors of colloids do not change when exposed to other analyte vapors (Figure 13). It is worth noting that, compared with the traditional solid substrate, sufficient space in the colloidal oligomers avoids the fluorescence self-quenching caused by the aggregation of spiropyran molecules. Solid state fluorescence spectra of SC-FSP@$Ca_3(PO_4)_2$ oligomer colloid are shown in Figure S13. The stimulus-responsive calcium ionic oligomer colloids containing spiropyrans are an alternative to complex equipment for the qualitative detection of gaseous hydrazine. It can be used to detect and continuously absorb hazardous vapors by simply applying the colloids to the leakage position in emergency situations, which avoids cumbersome experiments and the use of complicated instruments.

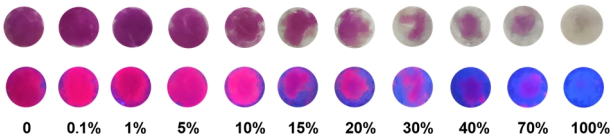

Figure 12. The color changes of colloidal SC-FSP@$Ca_3(PO_4)_2$ oligomers used for naked-eye detection of gaseous hydrazine. Upper row: visual color observed under ambient visible light. Lower row: fluorescent color observed under UV light.

Scheme 2 shows a plausible detection mechanism of SC-FSP for hydrazine, suggesting the fundamental reason is that the formation of hydrazone affects the absorption spectra and fluore-

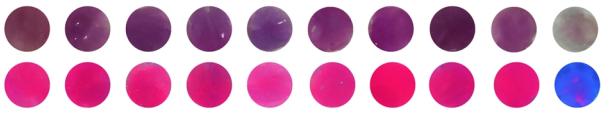

Figure 13. The color changes of colloidal SC-FSP@$Ca_3(PO_4)_2$ oligomers after exposure to different gaseous (blank, carbamide, isopropanolamine, ethylenediamine, ethanolamine, ammonium carbonate, dimethylamine, 1,2-propanediamine, hydrogen peroxide and hydrazine). Upper row: visual color observed under ambient visible light. Lower row: fluorescent color observed under UV light.

DOI: 10.14102/j.cnki.0254-5861.2022-0061

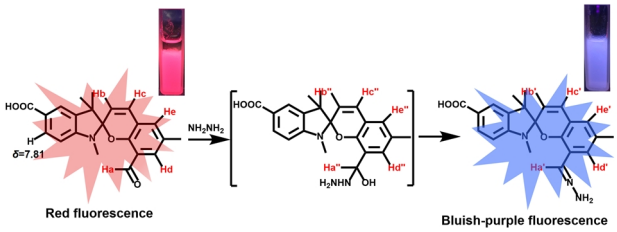

Scheme 2. Probable detection mechanism of SC-FSP toward N_2H_4.

scence signal of probe molecules. Mass spectrometry and NMR spectroscopy confirmed the formation of the key hemiaminal intermediates during the acylation reaction of hydrazine with formyl. The final product hydrazone was generated after removing a water molecule from the hemiaminal intermediate, while the SC-FSP still existed stably in the ring-closed SP form throughout the reaction process. The ^{1}H NMR titration spectra of SC-FSP and hydrazine in DMSO-d_6 at room temperature are exhibited in Figure 14. The peak at δ = 9.94 ppm is attributed to the formyl proton (-CHO, Ha) of probe SC-FSP. However, with the increase of hydrazine concentrations, the signal of proton Ha gradually diminishes until disappears with the addition of 0.7 equiv. hydrazine. While a new peak gradually appears at δ = 7.54 ppm, which is associated with the azomethine proton (CHa′=N)[43] of the product hydrazone. Since the formation of C=N affects the charge distribution, the chemical shift of the double bond proton Hb on the pyran ring shifts from 5.93 to 5.76 ppm (Hb′), and the peak of proton Hc also shifts from 7.10 to 6.97 ppm (Hc′). It can be found from the ^{1}H NMR spectra that two new bimodal signals of protons Hb" and Hc" appear at 5.84 and 7.03 ppm with the addition of 0.1 equiv. hydrazine, while the peaks of protons Hb′ and Hc′ in product hydrazone appear only when the amount of hydrazine increases to 0.3 equiv.. As the amount of hydrazine increases, the integration values of signals Hb" and Hc" first increase and then decrease, and the maximum values appear in the middle, while the signal intensities of product hydrazone Hb′ and Hc′ always increase to the maximum values during titration (Figure S14). Note that both the total integration values of Hb, Hb" and Hb′ and the total integration values of Hc, Hc" and Hc′ are approximately “1”. Therefore, we speculate that hemiaminal intermediate is formed before the

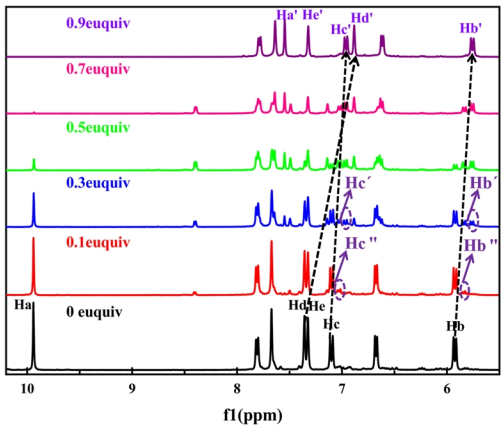

Figure 14. ^{1}H NMR spectra of SC-FSP (lowest) and the product of SC-FSP reacting with different equivalent N_2H_4 (solvent: DMSO-d_6).

hydrazone when 0.1 equiv. hydrazine is added. The integration values also confirm three proportional proton signal systems in the titration, which are raw materials SC-FSP, hemiaminal intermediates and final product hydrazone, respectively (Table S3). The existence of hemiaminal intermediate is also confirmed by the ^{13}C NMR titration spectra and mass spectrometry (Figure S15). It can be found that the signal peak in ^{13}C NMR corresponding to formyl group at 188.05 ppm shifts to 125.45 ppm with the increase of hydrazine, which is consistent with the signal of azomethine (C=N) in the hydrazone. The signal peak of tertiary carbon (-CHOHNH-) of the hemiamine intermediate appears at 56.60 ppm with the addition of 0.1 equiv. hydrazine. The HRMS analysis (Figure S16) also demonstrates that the SC-FSP and hemiamine intermediate exist simultaneously when the probe reacts with 0.1 equiv. hydrazine, showing peaks at m/z = 362.1397 and m/z = 394.1692, respectively. With the increase of hydrazine equivalent, the signal peak of product hydrazone is obtained at m/z = 376.2 (Figure S17). To further ensure the accuracy of the NMR spectra of semiamine intermediate and product hydrazone, the geometric optimizations and vibrational frequencies were performed at the DFT level with the B3LYP functional and 6-31+G (d, p) basis set by Gaussian 09 software. Based on the optimized geometry, the magnetic shielding tensors were calculated by mPW1PW91/6-311+G (2d, p) method. It can be found that the experimental values of the chemical shifts of hydrogen and carbon atoms are basically consistent with the calculated ones (Tables S4 and 5). On the basis of the above experiments, it is confirmed that the detection mechanism is the acylation reaction of hydrazine toward formyl with semiamine compounds as intermediates, and finally the product hydrazone is obtained, resulting in the changes of fluorescence and absorption spectra.

n CONCLUSION

In conclusion, we report a general strategy for the immobilization of spiropyrans via calcium ionic oligomers. In addition to being involved in the formation of oligomers, Ca^{2+} is also used to regulate the optical properties of spiropyrans through chelation to achieve reversible positive photochromism. Compared with the solid substrate, the colloidal oligomers not only provide the space required for its photoisomerization, but also avoid the interference of the surrounding environment of spiropyran molecules in the solutions on their photochromic properties, so that the spiropyrans embedded in the oligomers have an acceptable environmental tolerance. The photochromic properties of spiropyrans go hand in hand with the oligomer states. Since the matrix density of spiropyrans is enhanced by centrifugation, the absorbance characteristic of MC is significantly higher in the oligomer colloids than that in original oligomers solution after UV excitation. The kinetic studies show that the steric hindrance is increased in the colloidal substrate, which enhances the thermal stability of the chromogenic MC. In addition, the calcium ionic oligomer colloids containing spiropyrans have potential applications in optical information storage, anti-counterfeiting technology and the naked-eye detection of hydrazine vapor. The spectroscopic studies and DFT calculations confirm that the detection mechanism is the acylation reaction of hydrazine and formyl with semiamine compounds as intermediates.

DOI: 10.14102/j.cnki.0254-5861.2022-0061

n EXPERIMENTAL

Materials and General Methods. Here, it should be noted that reagents and solvents obtained from commercial suppliers were directly used without further purification. Compound B was synthesized according to the reported procedures.[44] Infrared spectra of compounds were recorded via a Nicolet Magna 750 FT-IR spectrometer with the wavenumber range of (4000-400) cm^{-1}. NMR spectra were performed on an INOVA-400 spectrometer with DMSO-d_6 as the solvent. Mass spectra were measured on an Exploris 480 detector instrument. Electronic absorption spectra and kinetic curves of the studied compounds were obtained on a UV759S spectrophotometer. The isomerization of ring-closed SP to ring-opened MC was stimulated by an ultraviolet lamp (365 nm, 15 W). Ordinary LED lamp that emitted white light provided the required visible light. Photoluminescent spectra were collected using F-7000 spectrofluorimeter. A few drops of diluted oligomer solution were placed on silicon wafer and dried at 50 °C for 1 hour in vacuum condition. Then elemental analysis (C, H, O, N, P, S, Ca) and microscopic topography observation of functionalized calcium phosphate and calcium sulfate oligomers were carried out by SEM-EDS (Hitachi S-4800, Japan). The X-ray photoelectron spectroscopy (XPS) was acquired on an AXIS SUPRA spectrometer (SHIMADZU, Japan) to analyze chemical composition and atomic valence states on the surface of the functionalized calcium sulfate.

Synthesis and Characterization of Spiropyrans. The synthesis of three spiropyrans are shown in Figure 15. DC-FSP:1,3,3-trimethyl-2-methyleneindoline-4,6-dicarboxylic acid (1.57 g, 6 mmol) and compound A (0.984 g, 6 mmol) were dissolved in 30 mL of a mixed solution of water and anhydrous ethanol (*V*:*V* = 1:1). The reaction solution was refluxed at 100 °C for 10 h, and then filtered under reduced pressure. The obtained crude mixture (black green) was stirred to re-dissolve in 30 mL of ethyl acetate and the solvent was then removed again by vacuum rotary evaporation. The resulting crude residue (black) was recrystallized from ethanol-water (*V*:*V* = 1:1) mixture to obtain an ocher solid DC-FSP (1.25 g, yield: 51.2%). HRMS: *m*/*z* calcd. $C_{23}H_{21}O_6N$ $(M+H)^+$: 408.14. ^1H NMR (400 MHz, DMSO): δ 9.89 (s, 1H), 7.77 (s, 1H), 7.37 (s, 1H), 7.33 (s, 1H), 7.26 (s, 1H), 7.15 (d, *J* = 10.3 Hz, 1H), 5.96 (d, *J* = 10.1 Hz, 1H), 2.78 (s, 3H), 2.26 (s, 3H), 1.39 (s, 3H), 1.34 (s, 3H). ^{13}C NMR (101 MHz, DMSO): δ 188.01, 168.75, 167.31, 155.08, 149.87, 139.94, 134.36, 130.97, 130.01, 129.75, 129.23, 127.56, 122.43, 121.90, 120.09, 119.82, 110.13, 106.36, 53.76, 29.61, 22.70, 20.24, 18.91.

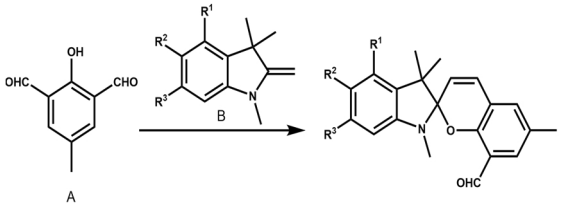

Figure 15. Synthesis of spiropyrans (FSP: R1 = R2 = R3 = H; SC-FSP: R1 = R3 = H, R2 = COOH; DC-FSP: R1 = R3 = COOH, R2 = H).

FSP: 1,3,3-trimethyl-2-methyleneindoline (1.142 g, 6.6 mmol) and compound A (0.984 g, 6 mmol) were dissolved in 40 mL of anhydrous ethanol, and the reaction solution was refluxed at 100 °C for 8 h. Then 20 mL of deionized water was added to the solution and stirred at room temperature for 20 min, and a brown gelatinous substance was precipitated. The crude residue was recrystallized from ethanol/water (*V*:*V* = 1:1) to obtain DSP as a reddish-brown solid (1.309 g, yield: 68.4%). HRMS: *m*/*z* calcd. $C_{21}H_{21}O_2N$ $(M+H)^+$: 320.16. ^1H NMR (400 MHz, DMSO): δ 9.95 (s, 1H), 7.33 (s, 2H), 7.13 (t, *J* = 7.7 Hz, 2H), 7.08 (d, *J* = 10.3 Hz, 1H), 6.81 (t, *J* = 7.3 Hz, 1H), 6.61 (d, *J* = 7.6 Hz, 1H), 5.91 (d, *J* = 10.3 Hz, 1H), 2.69 (s, 3H), 2.24 (s, 3H), 1.26 (s, 3H), 1.13 (s, 3H). ^{13}C NMR (101 MHz, DMSO): δ 188.80, 156.13, 148.69, 137.30, 135.06, 130.37, 129.96, 128.78, 128.03, 122.75, 122.71, 121.62, 121.27, 120.50, 108.17, 106.25, 52.82, 29.83, 26.81, 25.33, 21.36, 21.04.

SC-FSP: 1,3,3-trimethyl-2-methyleneindoline-5-carboxylic acid (1.432 g, 6.6 mmol) and compound A (0.984 g, 6 mmol) were dissolved in 30 mL of a mixed solution of water and anhydrous ethanol (*V*:*V* = 1:1). The reaction solution was refluxed at 100 °C for 8 h and cooled to room temperature. The precipitate was filtered and washed with water to obtain a yellow powdery SC-FSP. (0.908 g, yield: 41.7%). HRMS: *m*/*z* calcd. $C_{22}H_{21}O_4N$ $(M+H)^+$: 364.41. ^1H NMR (400 MHz, DMSO): δ 9.97 (s, 1H), 7.84 (d, *J* = 8.2 Hz, 1H), 7.71 (s, 1H), 7.37 (d, *J* = 10.5 Hz, 2H), 7.12 (d, *J* = 10.2 Hz, 1H), 6.71 (d, *J* = 8.2 Hz, 1H), 5.95 (d, *J* = 10.4 Hz, 1H), 2.79 (s, 3H), 2.27 (s, 3H), 1.31 (s, 3H), 1.17 (s, 3H). ^{13}C NMR (101 MHz, DMSO) δ 188.86, 168.71, 155.62, 152.51, 137.36, 135.13, 132.06, 130.72, 130.21, 128.38, 124.11, 122.89, 122.67, 121.07, 121.04, 107.43, 106.11, 52.54, 29.71, 21.31, 21.07.The corresponding spectra are shown in Figure S18-26.

Synthesis and Characterization of Spiropyran Calcium Ionic Oligomers.

Synthesis of DC-FSP@$(Ca_3(PO_4)_2)_n$ Oligomer. Firstly, 0.0832 g anhydrous calcium chloride was dissolved in 15 mL anhydrous ethanol to yield a solution containing 30 mM Ca^{2+}. Secondly, 10 mL ethanol solution containing 10 mM H_3PO_4 with 300 mM triethylamine was prepared. Subsequently, the two solutions were quickly mixed and were added a certain concentration of DC-FSP ethanol solution in drops. The mixing solution was stirred for 30 min to generate a translucent solution containing DC-FSP@$(Ca_3(PO_4)_2)_n$ oligomer, which was called as the initial DC-FSP@$(Ca_3(PO_4)_2)_n$ oligomer solution. Colloidal oligomers DC-FSP@$(Ca_3(PO_4)_2)_n$ were finally collected by centrifugation (1600 rpm, 25 °C, 10 min) of their oligomer solution. The preparation of SC-FSP@$(Ca_3(PO_4)_2)_n$ and FSP@$(Ca_3(PO_4)_2)_n$ oligomers was similar to the above method, except that the type of spiropyrans was changed. SC-FSP[45] and FSP[46] were successfully synthesized according to previous reports.

Synthesis of SC-FSP@$(CaSO_4)_n$ oligomer. 15 mL EtOH solution including 30 mM Ca^{2+} and 10 mL EtOH solution including 15 mM H_2SO_4 with 300 mM TEA were prepared. Then, the two solutions were quickly mixed, to which an ethanol solution of SC-FSP was added in drops. After stirring for half an hour, the suspension

DOI: 10.14102/j.cnki.0254-5861.2022-0061

was centrifuged to finally obtain SC-FSP@$(CaSO_4)_n$ colloidal oligomers.

n ACKNOWLEDGEMENTS

This work was supported by the National Natural Science Foundation of China (Nos. 21173074 and 112074322) and the Natural Science Foundation of Hunan Province (No. 2018JJ2034).

n AUTHOR INFORMATION

Corresponding authors. Emails: ychen@hnu.edu.cn (Yun Chen) and liuxy@xmu.edu.cn (Xiangyang Liu)

n COMPETING INTERESTS

The authors declare no conflict of interest.

n ADDITIONAL INFORMATION

Supplementary information is available for this paper at http://manu30.magtech.com.cn/jghx/EN/10.14102/j.cnki.0254-5861.2022-0061

For submission: https://mc03.manuscriptcentral.com/cjsc

n REFERENCES

(1) Zhang, X.; Zhang, J.; Ying, Y. L.; Tian, H.; Long, Y. T. Single molecule analysis of light-regulated RNA: spiropyran interactions. *Chem. Sci.* **2014**, 5, 2642-2646.

(2) Wang, J. X.; Li, C.; Tian, H. Energy manipulation and metal-assisted photochromism in photochromic metal complex. *Coord. Chem. Rev.* **2021**, 427, 213579.

(3) Julià-López, A.; Hernando, J.; Ruiz-Molina, D.; González-Monje, P.; Sedó, J.; Roscini, C. Temperature-controlled switchable photochromism in solid materials. *Angew. Chem. Int. Ed.* **2016**, 55, 15044-15048.

(4) Euchler, D.; Ehgartner, C. R.; Hüsing, N.; Feinle, A. Monolithic spiropyran-based porous polysilsesquioxanes with stimulus-responsive properties. *ACS Appl. Mater. Interfaces* **2020**, 12, 47754-47762.

(5) Yang, R.; Ren, X.; Mei, L.; Pan, G.; Li, X.; Wu, Z.; Zhang, S.; Ma, W.; Yu, W.; Fang, H. Reversible three-color fluorescence switching of an organic molecule in the solid state via “pump-trigger” optical manipulation. *Angew. Chem. Int. Ed.* **2022**.

(6) Julià-López, A.; Ruiz-Molina, D.; Hernando, J.; Roscini, C. Solid materials with tunable reverse photochromism. *ACS Appl. Mater. Interfaces* **2019**, 11, 11884-11892.

(7) Gao, Y.; Yin, Q.; Geng, X.; Zhang, X.; Li, W.; Gao, Y.; Geng, X.; Zhang, X.; Li, W. Synthesis and photochromic behavior of comb-like acrylate polymer nanoparticle containing spiropyran. *Dyes Pigments* **2021**, 189, 109237.

(8) Abdollahi, A.; Sahandi-Zangabad, K.; Roghani-Mamaqani, H. Rewritable anticounterfeiting polymer inks based on functionalized stimuli-responsive latex particles containing spiropyran photoswitches: reversible photopatterning and security marking. *ACS Appl. Mater. Interfaces* **2018**, 10, 39279-39292.

(9) Qiu, W.; Gurr, P. A.; Qiao, G. G. Color-switchable polar polymeric materials. *ACS Appl. Mater. Interfaces* **2019**, 11, 29268-29275.

(10) Williams, D. E.; Martin, C. R.; Dolgopolova, E. A.; Swifton, A.; Godfrey, D. C.; Ejegbavwo, O. A.; Pellechia, P. J.; Smith, M. D.; Shustova, N. B. Flipping the switch: fast photoisomerization in a confined environment. *J. Am. Chem. Soc.* **2018**, 140, 7611-7622.

(11) Kremer, S.; Ober, I.; Greussing, V.; Kopacka, H.; Gallmetzer, H. G.; Trubenbacher, B.; Demmel, D.; Olthof, S.; Huppertz, H.; Schwartz, H. A. Modulating the optical characteristics of spiropyran@metal-organic framework composites as a function of spiropyran substitution. *Langmuir* **2021**, 37, 7834-7842.

(12) Rice, A. M.; Martin, C. R.; Galitskiy, V. A.; Berseneva, A. A.; Leith, G. A.; Shustova, N. B. Photophysics modulation in photoswitchable metal-organic frameworks. *Chem. Rev.* **2020**, 120, 8790-8813.

(13) Liang, H. Q.; Guo, Y.; Shi, Y.; Peng, X.; Liang, B.; Chen, B. A light-responsive metal-organic framework hybrid membrane with high on/off photoswitchable proton conductivity. *Angew. Chem. Int. Ed.* **2020**, 59, 7732-7737.

(14) Garg, S.; Schwartz, H.; Kozlowska, M.; Kanj, A. B.; Müller, K.; Wenzel, W.; Ruschewitz, U.; Heinke, L. Lichtinduziertes Schalten der Leitfähigkeit von MOFs mit eingelagertem Spiropyran. *Angew. Chem.* **2019**, 131, 1205-1210.

(15) Kundu, P. K.; Olsen, G. L.; Kiss, V.; Klajn, R. Nanoporous frameworks exhibiting multiple stimuli responsiveness. *Nat. Commun.* **2014**, 5, 1-9.

(16) Martin, C. R.; Park, K. C.; Corkill, R. E.; Kittikhunnatham, P.; Leith, G. A.; Mathur, A.; Abiodun, S. L.; Greytak, A. B.; Shustova, N. B. Photoresponsive frameworks: energy transfer in the spotlight. *Faraday Discuss.* **2021**, 231, 266-280.

(17) Mohan Raj, A.; Raymo, F. M.; Ramamurthy, V. Reversible disassembly-assembly of octa acid-guest capsule in water triggered by a photochromic process. *Org. Lett.* **2016**, 18, 1566-1569.

(18) Zhang, X. F.; Ma, X.; Hou, T.; Guo, K.; Yin, J.; Wang, Z.; Shu, L.; He, M.; Yao, J. Inorganic salts induce thermally reversible and anti-freezing cellulose hydrogels. *Angew. Chem. Int. Ed.* **2019**, 58, 7366-7370.

(19) Zhang, H.; Dasbiswas, K.; Ludwig, N. B.; Han, G.; Lee, B.; Vaikuntanathan, S.; Talapin, D. V. Stable colloids in molten inorganic salts. *Nature* **2017**, 542, 328-331.

(20) El Sayed, S.; Pascual, L. S.; Licchelli, M.; Martínez-Máñez, R.; Gil, S.; Costero, A. M.; Sancenón, F. l. Chromogenic detection of aqueous formaldehyde using functionalized silica nanoparticles. *ACS Appl. Mater. Interfaces* **2016**, 8, 14318-14322.

(21) Wang, Z.; Wang, W.; Sun, G.; Yu, D. Designed ionic microchannels for ultrasensitive detection and efficient removal of formaldehyde in an aqueous solution. *ACS Appl. Mater. Interfaces* **2019**, 12, 1806-1816.

(22) Bruemmer, K. J.; Green, O.; Su, T. A.; Shabat, D.; Chang, C. J. Chemiluminescent probes for activity-based sensing of formaldehyde released from folate degradation in living mice. *Angew. Chem. Int. Ed.* **2018**, 57, 7508-7512.

(23) Ma, X.; Tang, K. l.; Lu, K.; Zhang, C.; Shi, W.; Zhao, W. Structural engineering of hollow microflower-like CuS@C hybrids as versatile electrochemical sensing platform for highly sensitive hydrogen peroxide and hydrazine detection. *ACS Appl. Mater. Interfaces* **2021**, 13, 40942-40952.

(24) Vernot, E. H.; MacEwen, J. D.; Bruner, R. H.; Haun, C. C.; Kinkead, E. R.; Prentice, D. E.; Hall Iii, A.; Schmidt, R. E.; Eason, R. L.; Hubbard, G. B. Long-term inhalation toxicity of hydrazine. *Fundam. Appl. Toxicol.* **1985**, 5, 1050-1064.

(25) Liu, Z.; Shao, C.; Jin, B.; Zhang, Z.; Zhao, Y.; Xu, X.; Tang, R. Cross-linking ionic oligomers as conformable precursors to calcium carbonate. *Nature* **2019**, 574, 394-398.

(26) Keyvan Rad, J.; Ghomi, A. R.; Karimipour, K.; Mahdavian, A. R. Progressive readout platform based on photoswitchable polyacrylic nanofibers

DOI: 10.14102/j.cnki.0254-5861.2022-0061

containing spiropyran in photopatterning with instant responsivity to acid-base vapors. *Macromolecules* **2020**, 53, 1613-1622.
(27) Qiu, X.; Ivasyshyn, V.; Qiu, L.; Enache, M.; Dong, J.; Rousseva, S.; Portale, G.; Stöhr, M.; Hummelen, J. C.; Chiechi, R. C. Thiol-free self-assembled oligoethylene glycols enable robust air-stable molecular electronics. *Nat. Mater.* **2020**, 19, 330-337.
(28) Grissa, R.; Abramova, A.; Tambio, S. J.; Lecuyer, M.; Deschamps, M.; Fernandez, V.; Greneche, J. M.; Guyomard, D.; Lestriez, B.; Moreau, P. Thermomechanical polymer binder reactivity with positive active materials for Li metal polymer and Li-ion batteries: an XPS and XPS imaging study. *ACS Appl. Mater. Interfaces* **2019**, 11, 18368-18376.
(29) Lu, Y.; Cai, Y.; Zhang, Q.; Ni, Y.; Zhang, K.; Chen, J. Rechargeable K-CO_2 batteries with a KSn anode and a carboxyl-containing carbon nanotube cathode catalyst. *Angew. Chem. Int. Ed.* **2021**, 60, 9540-9545.
(30) Eckhardt, H.; Bose, A.; Krongauz, V. A. Formation of molecular H- and J-stacks by the spiropyran-merocyanine transformation in a polymer matrix. *Polymer* **1987**, 28, 1959-1964.
(31) Nakamura, M.; Fujioka, T.; Sakamoto, H.; Kimura, K. High stability constants for multivalent metal ion complexes of crown ether derivatives incorporating two spirobenzopyran moieties. *New J. Chem.* **2002**, 26, 554-559.
(32) Tanaka, M.; Ikeda, T.; Xu, Q.; Ando, H.; Shibutani, Y.; Nakamura, M.; Sakamoto, H.; Yajima, S.; Kimura, K. Synthesis and photochromism of spirobenzopyrans and spirobenzothiapyran derivatives bearing monoazathiacrown ethers and noncyclic analogues in the presence of metal ions. *J. Org. Chem.* **2002**, 67, 2223-2227.
(33) Lin, S.; Ruan, Y. Z.; Shen, Y.; Luo, J. R. Crystalline phase and decomposition dynamics of aluminum titanate at different temperature. *Chin. J. Struct. Chem.* **2012**, 31, 79-84.
(34) Abdollahi, A.; Roghani-Mamaqani, H.; Razavi, B.; Salami-Kalajahi, M. Photoluminescent and chromic nanomaterials for anticounterfeiting technologies: recent advances and future challenges. *ACS Nano* **2020**, 14, 14417-14492.
(35) Li, X.; Xu, S.; Liu, F.; Qu, J.; Shao, H.; Wang, Z.; Cui, Y.; Ban, D.; Wang, C. Bi and Sb codoped $Cs_2Ag_{0.1}Na_{0.9}InCl_6$ double perovskite with excitation-wavelength-dependent dual-emission for anti-counterfeiting application. *ACS Appl. Mater. Interfaces* **2021**, 13, 31031-31037.
(36) Wang, F.; Gerken, J. B.; Bates, D. M.; Kim, Y. J.; Stahl, S. S. Electrochemical strategy for hydrazine synthesis: development and overpotential analysis of methods for oxidative N-N coupling of an ammonia surrogate. *J. Am. Chem. Soc.* **2020**, 142, 12349-12356.
(37) Jia, Y.; Shang, N.; He, X.; Nsabimana, A.; Gao, Y.; Ju, J.; Yang, X.; Zhang, Y. Electrocatalytically active cuprous oxide nanocubes anchored onto macroporous carbon composite for hydrazine detection. *J. Colloid Interface Sci.* **2022**, 606, 1239-1248.
(38) García-Aldea, D.; Alvarellos, J. E. Generalized nonlocal kinetic energy density functionals based on the von Weizsäcker functional. *PCCP* **2012**, 14, 1756-1767.
(39) Li, J.; Yim, D.; Jang, W. D.; Yoon, J. Recent progress in the design and applications of fluorescence probes containing crown ethers. *Chem. Soc. Rev.* **2017**, 46, 2437-2458.
(40) Feller, D.; Bross, D. H.; Ruscic, B. Enthalpy of formation of N_2H_4 (hydrazine) revisited. *J. Phys. Chem. A* **2017**, 121, 6187-6198.
(41) Fabiano, B.; Reverberi, A. P.; Varbanov, P. S. Safety opportunities for the synthesis of metal nanoparticles and short-cut approach to workplace risk evaluation. *J. Clean. Prod.* **2019**, 209, 297-308.
(42) Liu, T.; Yang, L. J.; Feng, W.; Liu, K.; Ran, Q.; Wang, W.; Liu, Q.; Peng, H.; Ding, L.; Fang, Y. Dual-mode photonic sensor array for detecting and discriminating hydrazine and aliphatic amines. *ACS Appl. Mater. Interfaces* **2020**, 12, 11084-11093.
(43) Kong, X.; Li, M.; Zhang, Y.; Yin, Y.; Lin, W. Engineering an AIE N_2H_4 fluorescent probe based on α-cyanostilbene derivative with large Stokes shift and its versatile applications in solution, solid-state and biological systems. *Sens. Actuators B Chem.* **2021**, 329, 129232.
(44) Guo, T.; Wu, J.; Gao, H.; Chen, Y. Covalent functionalization of multi-walled carbon nanotubes with spiropyran for high solubility both in water and in non-aqueous solvents. *Inorg. Chem. Commun.* **2017**, 83, 31-35.
(45) Ozhogin, I. V.; Chernyavina, V. V.; Lukyanov, B. S.; Malay, V. I.; Rostovtseva, I. A.; Makarova, N. I.; Tkachev, V. V.; Lukyanova, M. B.; Metelitsa, A. V.; Aldoshin, S. M. Synthesis and study of new photochromic spiropyrans modified with carboxylic and aldehyde substituents. *J. Mol. Struct.* **2019**, 1196, 409-416.
(46) Goswami, S.; Aich, K.; Das, S.; Das, A. K.; Sarkar, D.; Panja, S.; Mondal, T. K.; Mukhopadhyay, S. A red fluorescence 'off-on' molecular switch for selective detection of Al^{3+}, Fe^{3+} and Cr^{3+}: experimental and theoretical studies along with living cell imaging. *Chem. Commun.* **2013**, 49, 10739-10741.

Received: March 18, 2022
Accepted: April 8, 2022
Published: May 20, 2022

DOI: 10.14102/j.cnki.0254-5861.2022-0061